THE ASTROPHYSICAL JOURNAL, 314:322–328, 1987 March 1

HIGH-RESOLUTION OBSERVATIONS OF CO FROM THE BIPOLAR NEBULA CRL 2688[1]

R. KAWABE, M. ISHIGURO, T. KASUGA, K.-I. MORITA, AND N. UKITA
Nobeyama Radio Observatory, Tokyo Astronomical Observatory, University of Tokyo

H. KOBAYASHI AND S. OKUMURA
Department of Astronomy, University of Tokyo

E. FOMALONT
Nobeyama Radio Observatory, Tokyo Astronomical Observatory, University of Tokyo; and National Radio Astronomy Observatory[2]

AND

N. KAIFU
Nobeyama Radio Observatory, Tokyo Astronomical Observatory, University of Tokyo
Received 1986 April 3; accepted 1986 August 26

ABSTRACT

We have mapped the CO emission from an expanding molecular envelope of the bipolar nebula CRL 2688 using the Nobeyama 45 m telescope with 15″ resolution. The CO spectrum toward the center shows line wings with a full width of 85 km s^{-1}. On the blueshifted wing, a narrow and deep absorption feature is seen at a velocity shifted by 20 km s^{-1} from the systemic velocity. The maps show three remarkable structures: a central compact core (0.05 pc × 0.1 pc) elongated perpendicularly to the bipolar axis, two spurs tracing the outer edge of the northern optical lobe, and blueshifted high-velocity emission distributed along the optical lobes.

The core and the high-velocity emission suggest the presence of the expanding disk of molecular gas and the fast stellar wind as acceleration agent, respectively. The spurs and the high-velocity emission of CO probably originate from the wind shells confined by the disk.

The absorption feature suggests that an expanding cold absorbing envelope surrounds the relatively warm molecular envelope. The absorbing envelope has an excitation temperature lower than about 5 K and an optical depth larger than 1.2 in CO(J = 1–0) line, and it is expanding at v = 20 km s^{-1}. The size of the absorbing envelope is estimated to be larger than 0.6 pc and the lower limit of its mass lies in the range (1.6–4.4) × 10^{-2} $M_\odot$.

Subject headings: interstellar: molecules — nebulae: individual — nebulae: reflection — stars: mass loss

I. INTRODUCTION

The reflection nebula CRL 2688 has a bipolar optical appearance (Ney *et al.* 1975). The central infrared source is a low-mass star with a spectral type of F5 (Crampton, Cowley, and Humphreys 1975). Radio molecular line observations have revealed an expanding dense molecular envelope ($V_{exp} \approx 20$ km s^{-1} and $M \approx 1\ M_\odot$) around the nebula (Zuckerman *et al.* 1976; Lo and Bechis 1976; Knapp *et al.* 1982; Thronson and Mozurkewich 1983; Nguyen-Q-Rieu, Graham, and Bujarrabal 1984). Beckwith, Persson, and Gatley (1978) have detected H_2 emission at 2.2 μm suggesting the presence of shocked gas. The H_2 emission was found to be emitted from each lobe of the bipolar nebula (Beckwith, Beck, and Gatley 1984).

It has been suggested that CRL 2688 is one of the proto–planetary nebulae which are at the stage in which the central star is evolving from a red giant star with rapid mass loss (Zuckerman 1978). The bipolar shape in both optical and H_2 emission indicates that a dense toroidal-shaped region of dust and gas surrounds the star and obscures optical emission. The toroid is probably responsible for channelling the mass loss to the polar directions (Ney *et al.* 1975; Morris 1981; Beckwith, Beck, and Gatley 1984). Observations which yield detailed information on the spatial and dynamical structure of the molecular gas are necessary for understanding the structure and origin of the bipolar nebula.

This paper reports the results of high spatial resolution mapping observations of CO emission from CRL 2688 using the Nobeyama 45 m telescope. We discuss the structure of the molecular envelope which is consistent with our observations and discuss the formation mechanism of bipolar nebula.

II. OBSERVATIONS

Observations of CO(J = 1–0) line were made on 1985 April 23 and 24 using the 45 m telescope of Nobeyama Radio Observatory with an HPBW of 15″ and a main beam efficiency of 0.3. We used a 115 GHz SSB Schottky diode mixer receiver cooled to 20 K, and an acoust-optical spectrometer with a frequency resolution of 250 kHz (0.65 km s^{-1}) and a bandwidth of 250 MHz (650 km s^{-1}). The system noise temperature at 115 GHz was measured to be 650 K at the zenith. Calibrations of antenna temperatures were made by the chopper wheel method, and the intensity scale reported here is the antenna temperature, T_A*, corrected for atmospheric and ohmic losses (Ulich and Haas 1976).

An initial scan ±1′ north and east of the central position showed that the CO emission was confined to ±30″ from the center. We thus mapped an area of 1′ × 1′ centered on the infrared source, R.A.(1950) = $21^h00^m19^s.9$, decl.(1950) =

[1] This work was carried out under the common use observation program at Nobeyama Radio Observatory (NRO). Nobeyama Radio Observatory, a branch of the Tokyo Astronomical Observatory, University of Tokyo, is a cosmic radio observing facility open for outside users.

[2] The National Radio Astronomy Observatory is operated by Associated Universities, Inc., under contract to the National Science Foundation.

+36°29′45″, using 81 positions at a grid spacing of 7″.5. Data were taken in a position switching mode with a fixed reference position at the 10′ east from the center. The grid inclined by 15° east of north, parallel to the major axis of the visible nebula (see Fig. 3*i*).

Each basic observation scan contained a 30 s integration at 10 positions; nine along the points on a parallel grid line and the tenth at the central point which was used to monitor the gain fluctuations in the system and small pointing offsets. The entire region of CRL 2688 was mapped with nine of these observation scans along the parallel grids; the mapping took about 60 minutes. Pointing calibrations were made before and after each set by observing the SiO(J = 1–0, v = 1) maser emission from NML Cyg, R.A.(1950) = $20^h44^m33^s.9$, decl.(1950) = +39°55′57″.0, which is about 4° apart from CRL 2688. The telescope pointing was determined to an accuracy of 2″–4″ and changes of about 4″ were applied on-line as the observations progressed. The source was mapped four times, two with scans in the direction parallel to the major axis and two, perpendicular to the major axis. This "basket-weaving" scheme was used in the reductions to reduce systematic offsets for each of the four mapping observations.

The typical rms noise temperature of spectra at each of the 81 points was 0.1 K at a velocity resolution of 2 km s^{-1} which was obtained by averaging three velocity channels.

III. RESULTS

Figure 1 shows a CO spectrum with 2 km s^{-1} resolution averaged for 30 spectra obtained toward the central infrared source in each scan (see § II). The intense part of the spectrum has a shape similar to that obtained by Thronson and Mozurkewich (1983). However, we have also detected broad wings with a full width of about 85 km s^{-1} and amplitude of 0.2 K. The wings are extended between V_{LSR} = 0 and V_{LSR} = −85 km s^{-1}, and the integrated intensity of the blue shifted part is about 2 or 3 times stronger than that of the redshifted part. The peak temperature of the spectrum, 2.2 K, leads to an excitation temperature, 10 K, assuming that the source size is sufficiently larger than the beam size and the CO line is fully optically thick. The temperature 10 K is actually a lower limit of the excitation temperature. It is slightly higher than that presented by Thronson and Mozurkewich (1983).

Figure 2 shows radial variation of CO spectra from the map center to the outer region; from the top to the bottom, a spectrum toward the center, and four spectra averaged for four annular regions with radii from the center position indicated in right upper corners of panels. The velocity resolution is 0.65 km s^{-1} for each spectrum. A deep and narrow absorption feature is seen at V_{LSR} = −55 km s^{-1} at the center position and marginally seen in the spectrum at the position (7″.5–11″). The feature has a velocity width of 1.3 km s^{-1} and T_A* at the bottom of 0.1–0.2 K, and the LSR velocity is blueshifted by 20 km s^{-1} from the line center. The feature is seen only on the blueshifted wing, and it is not present in the spectra obtained toward the outer region of the envelope. There are no obvious observational effects which could cause the feature, and we believe that it is real.

Figure 3 shows maps of the integrated intensity at seven

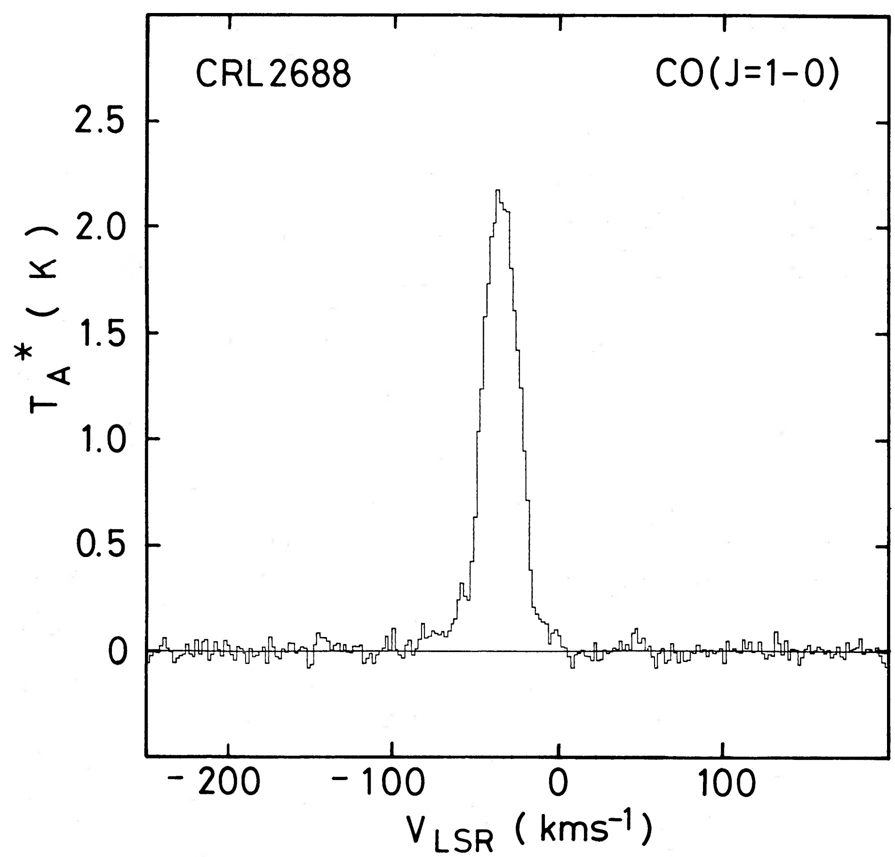

FIG. 1.—The ^{12}CO(J = 1–0) spectrum at the location of the central infrared source CRL 2688. The spectrum is an average of 30 observations with a total integration time of 20 minutes.

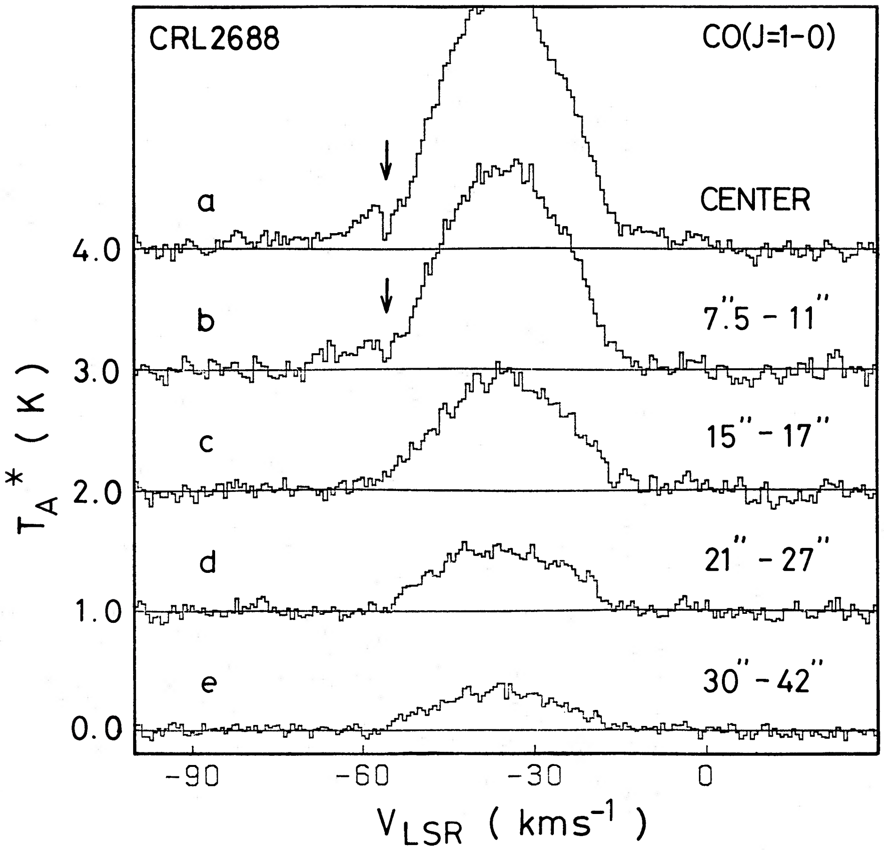

FIG. 2.—Radial variation of CO spectra from the center to the outer region with 0.65 km s^{-1} resolution. From top to bottom, (*a*) a spectrum toward the center, and four spectra averaged for four annuli with radii of (*b*) 7.″5–11″, (*c*) 15″–20″, (*d*) 21″–27″, and (*e*) 30″–42″. Two arrows indicate positions of the -55 km s^{-1} self-absorption dip.

radial velocities ([*a*]–[*g*]) each with 10 km s^{-1} integrated velocity width. The contour intervals on all maps is 1 K km s^{-1}. Figure 4 shows maps with different velocity ranges to better show aspects of the emission. The most important features seen on the maps are (1) a central compact core with an elongated shape and a circular 30″ component (maps 3*c*–3*e* and map 4*a*), (2) two spurs directed to the north (maps 3*b*–3*d* and map 4*c*), and (3) a blueshifted high-velocity CO emission with compact distribution (maps 3*a* and 4*b*).

The compact core is best seen near -45 km s^{-1} (maps 3*d* and 4*c*) and is centered near the infrared source. The core has a peak of about 7 K km s^{-1} at -35 km s^{-1} velocity. It is unresolved north-south ($\leq 10''$) and about 20″–25″ east-west. It corresponds to linear scales of 0.05 pc and 0.1–0.13 pc, respectively, assuming a distance of 1 kpc (Crampton, Cowley, and Humphreys 1975). The elongation of the central core is more remarkable at the blueshifted velocity that at the redshifted velocity, as seen in maps 3*b*, 3*c*, and 4*c*, and it corresponds very well to the direction of the central optically obscured region which has been interpreted as a dust disk surrounding the central star (see map 4*c*). The circular component, seen on maps 3*c*–3*e*, has a peak of about 14 K km s^{-1} at -35 km s^{-1}. The FWHM size of this component is about 30″.

At distances of more than 20″ from the center, low-level spurs of CO emission are apparent. At a velocity of about -70 km s^{-1} to -40 km s^{-1} two spurs in position angle $-10°$ are seen in maps 3*b*–3*d*. Weaker counterparts of these spurs are probably present to the south of the source (maps 3*c*–3*e* and 4*a*). The northern spurs roughly trace the outer edge of the optical northern lobe and might surround the lobe. Separations between the spurs are slightly different with velocity. In maps 3*d* and 3*e*, the separation is larger than that in map 3*c*.

There appears to be asymmetry in the high-velocity features near the source. The blueshifted emission is stronger than the redshifted emission, especially for velocities more than 25 km s^{-1} from the systemic velocity of the source. The blueshifted high-velocity emission is elongated along the bipolar axis and perpendicular to the compact core (see maps 4*b* and 4*c*). It is localized near the center, and the size of the emission region, 15″ × 25″ (0.075 pc × 0.125 pc), is comparable with that of the visible nebula. Corresponding redshifted emission at $V_{LSR} = -5$ km s^{-1} is very weak and cannot be seen in map 3*g*.

Figure 5 shows a radial distribution of the integrated intensity of CO emission between velocities -90 km s^{-1} and 10 km s^{-1}. All observed positions are plotted and logarithmic scales in radius and intensity have been used. Most of the CO emission from CRL 2688 is confined to the core with a radius of 10″–13″, and the remaining CO emission is extended up to 1′ (0.3 pc) from the center. The extended emission is not due to the sidelobe response of the telescope beam to the intense core, because the extended emission is larger by a factor of 2–4 than that expected for the sidelobe response. The envelope, therefore, is extending over 1′ (0.3 pc) from the center. Results of CO(J = 2–1) observations with a 26″ resolution also indicates

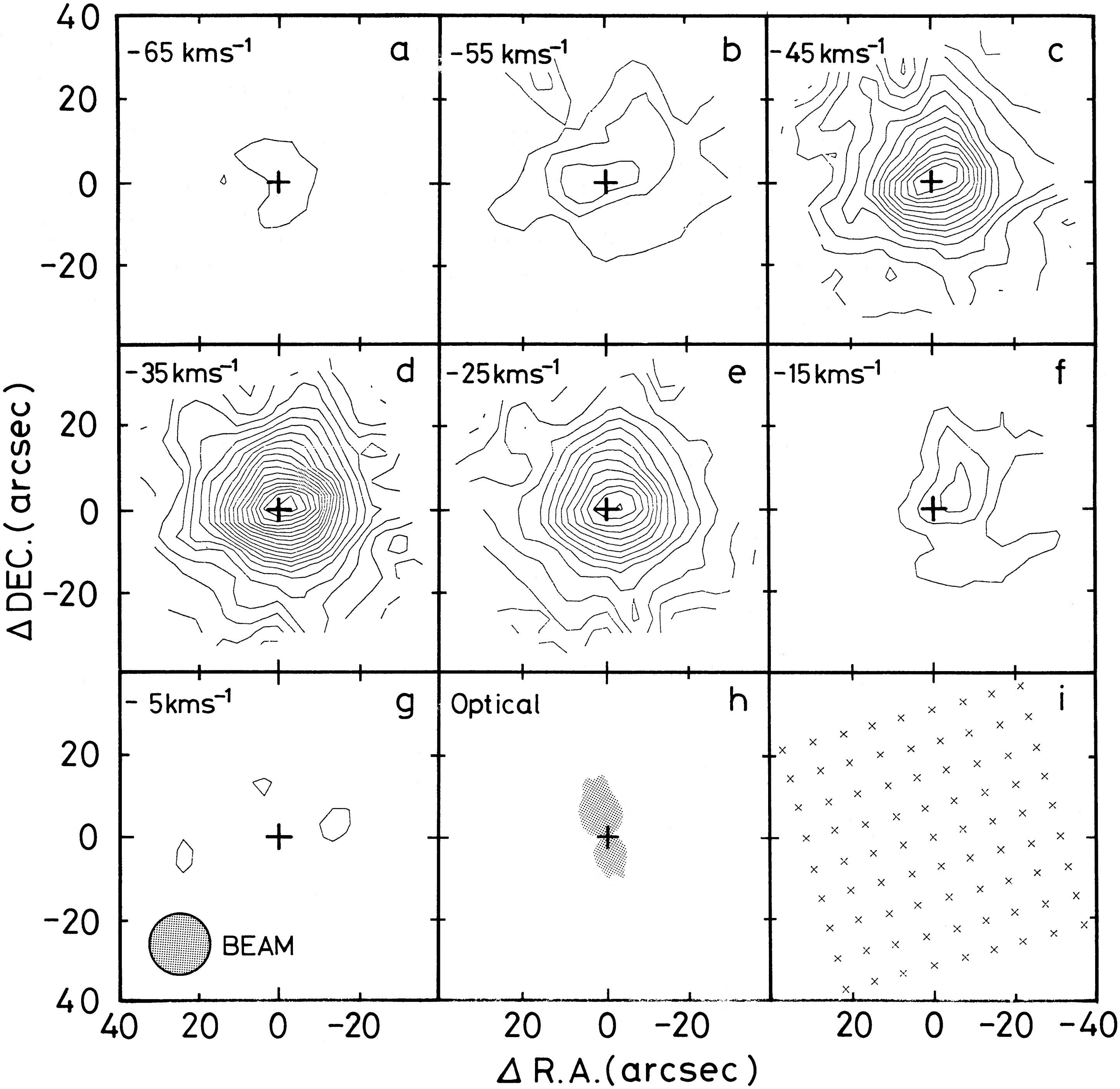

FIG. 3.—Maps of integrated intensity for seven velocity intervals with a velocity width of 10 km s^{-1}. A 15″ beam width, a schematic drawing of the optical appearance of CRL 2688, and observed grid are shown in panels (*g*), (*h*), and (*i*), respectively. The cross indicates the position of the infrared source, R.A.(1950) = $21^h00^m19^s.9$, decl.(1950) = $+36°29'45''$. Contour intervals are 1.0 K km s^{-1} for all the maps and the highest contour levels are 1.0, 3.0, 14.0, 21.0, 14.0, 3.0, and 1.0 for panels (*a*), (*b*), (*c*), (*d*), (*e*), (*f*), and (*g*), respectively.

that the CO distribution is extended (Knapp *et al.* 1982). The radial distribution well fits a power-law relation with an exponent of -1.3 ± 0.1 between 8″ and 60″. The scatter of the integrated intensity at each annular region is caused by the departures from the circular symmetry in the molecular envelope and measurement errors. However, the goodness of fit shows that a majority of the CO emission is distributed in a circularly symmetric region around the source.

IV. DISCUSSION

a) Model of CRL 2688

We discuss a possible model of CRL 2688 to account for our observational results. The schematic diagram of the model is shown in Figure 6.

The elongated compact core is small scale and related to the mass flow along the equatorial plane perpendicular to the

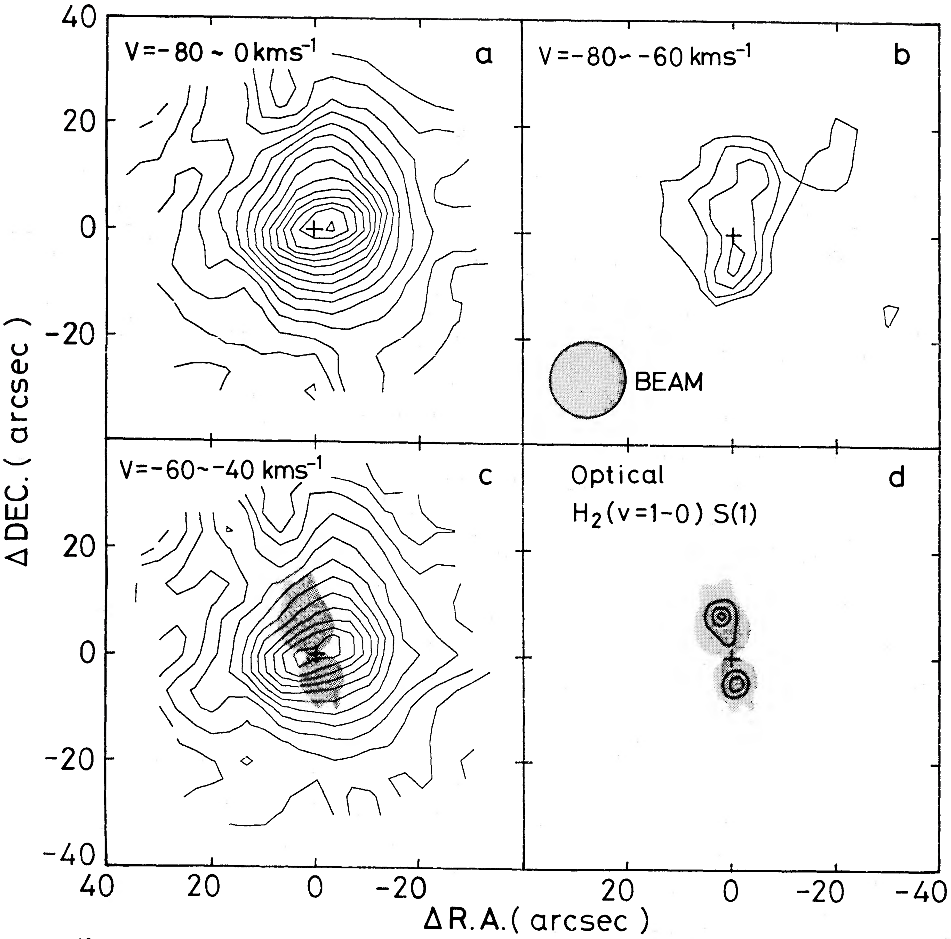

FIG. 4.—(*a*) A map of a total T_A*(^{12}CO) integrated intensity, (*b*) a map of partially integrated intensity between $V_{LSR} = -80$ and -60 km s^{-1}, (*c*) a map between $V_{LSR} = -60$ and -40 km s^{-1}, and (*d*) a schematic drawing of the optical appearance of CRL 2688 (*hatched region*) and H_2 (v = 1–0) S(1) emission (*contours*) (Beckwith *et al.* 1984). Contour intervals and the highest contour levels are 5.0, 0.5, and 1.0 K km s^{-1} and 60.0, 2.0, 18.0 K km s^{-1} for (*a*), (*b*), and (*c*), respectively.

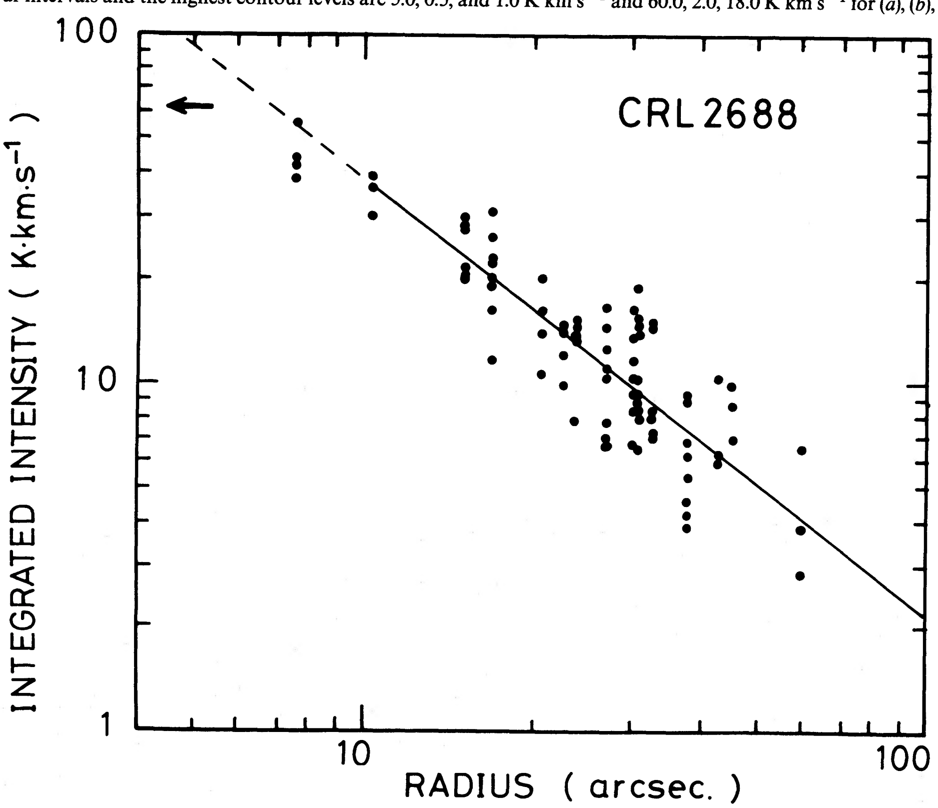

FIG. 5.—CO emission profile vs. radius in arcsec for the CO intensity integrated between $V_{LSR} = -90$ and 10 km s^{-1}. The data are plotted with logarithmic scales, and a least-squares fitted line using a power-law relation is shown. The power index is derived to be -1.3 ± 0.1. The arrow indicates the intensity of the center at the vertical axis.

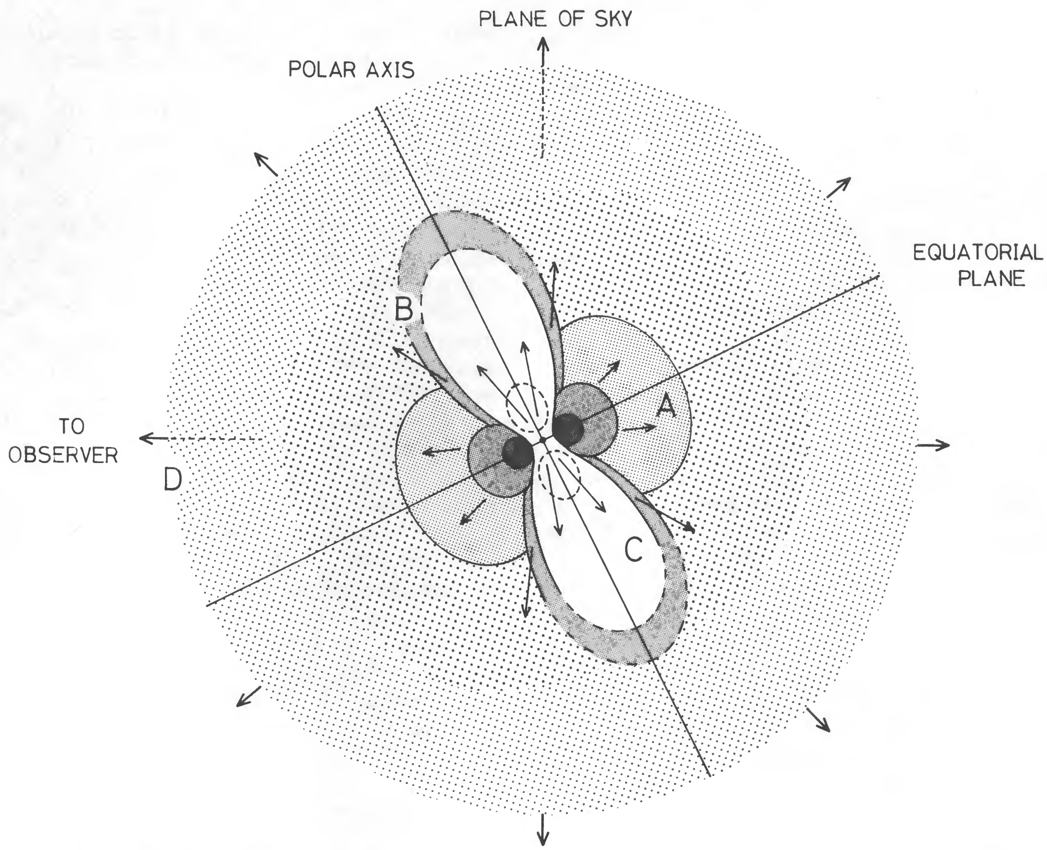

FIG. 6.—A model of CRL 2688. The structure has rotational symmetry about the bipolar axis. Four regions of the molecular envelope are indicated by the symbols A, B, C, and D. Region A is the expanding disk located at the equatorial plane. Region B indicates the expanding shells elongated to the polar directions. Region C is wind cavities interior to region B. Region D is the cold expanding envelope surrounding the warm envelope and causing the self-absorption. The arrows show the presumed outward radial flow of molecular gas. The optical reflection nebulae are indicated by the regions enclosed by dashed lines.

bipolar axis in region A. The circular 30″ CO emission represents material expanding after its flow out along the plane. The flow has the form of a compact expanding disk of molecular gas which surrounds the central infrared source and located on the equatorial plane.

The spurs to the north and to the south are a part of high-velocity flow in region B around the cavity C. The high-velocity flow has shell structures surrounding the optical lobes. At the tangential direction, the shells are seen as the northern two spurs. At the front side of the north shell, line-of-sight velocity is large and the shell is detected as the high velocity flow at the blueshifted side. The northern two spurs are prominents because the back side corresponds to the south, redshifted part.

The expansion motion of the shell explains the variation of the separation of the northern spurs which can be seen according to the change of the LSR velocity.

The high-velocity flow of molecular gas to the polar direction is caused by the disk geometry of molecular gas formed from the material shed by the central star. The fast stellar wind from the central star (Beckwith, Beck, and Gatley 1984) which is responsible for the gas acceleration interacts with the expanding disk because of velocity difference. This leads to the formation of a shock wave and shock-compressed shells. The stellar wind is isotropic in its initial stage, but the shock wave propagates anisotropically because of the disk. The envelope of the shock front elongates and expands to the polar directions of the disk (cf. Sakashita, Hanami, and Umemura 1985). The shells (region B) and cavities (region C) are formed by sweeping out molecular gas, and the shocks are induced at the cavity wall.

The bipolar appearance of the reflection nebula is a direct evidence of existence of the cavities. Optical emission from the star going through freely through the cavities is reflected at the surface of the walls and forms the bipolar optical appearance. Highly polarized optical emission with a position angle normal to the lobes (Ney *et al.* 1975) supports the reflection by the surface of the walls running parallel with the optical lobes. In addition, extinction by the disk plays a part to form the remarkable bipolar shape.

The flow to the polar directions (region B) has an extremely high velocity (~ 100 km s^{-1}) because the inclination angle of the optical lobe is supposed to be smaller than 30°. The dynamical time scale of the CO flow is estimated to be about 10^3 yr with an expanding velocity of 80 km s^{-1} and with an extent of the emissions of 0.08 pc (15″) from the center. The high velocity suggests the presence of a fast stellar wind for acceleration which is also suggested from the detection of the H_2 emission (Beckwith, Beck, and Gatley 1984).

The mass of the flow is estimated to be $2.3 \times 10^{-3}\ M_\odot$ for an optically thin case by assuming that the excitation temperature is the same as that at the line center, 10 K, and the abundance ratio of CO molecule to H_2 molecule, (CO)/(H_2), is 8×10^{-4} (Knapp and Morris 1985), the integrated velocity width is 85 km s^{-1}, and the emission region is about 15″ × 15″. The mass-loss rate is obtained to be $3 \times 10^{-6}\ M_\odot$ yr^{-1} which corresponds to a fraction of about 0.02 of a total mass-loss rate of the molecular envelope, $1.4 \times 10^{-4}\ M_\odot\ \mathrm{yr}^{-1}$ (Knapp and Morris 1985). The mass and the mass-loss rate derived here give lower limits and are probably underestimated because the emission is assumed to be optically thin.

b) Self-Absorption Feature at -55 km s^{-1}

The -55 km s^{-1} absorption feature seen only in the blueshifted wing implies the presence of an absorbing foreground cloud located between the observer and the high-velocity emission region. The absorption profile with a very narrow width suggests that the cloud may be quiescent isolated cloud not related to the envelope. But the situation is not acceptable from a kinematical point of view, because it is very unlikely that the isolated cloud with $V_{\mathrm{LSR}} = -55$ km s^{-1} is located between the Sun and CRL 2688 with a distance, 1 kpc, toward the direction at $(l, b) = (80°, -6°.5)$. The radial velocity expected from the galactic differential rotation in this region is 0–20 km s^{-1}. Then the absorbing cloud is very probably the outer cold envelope expanding from the central molecular envelope (region D in Fig. 6). This situation is supported by the fact that the LSR velocity of the absorbing cloud agrees with that of the envelope proceeding toward the observer with the expanding velocity of 20 km s^{-1} in CRL 2688. The self-absorption feature is easily reproduced by a model with excitation-temperature variation across the envelope (Morris, Lucas, and Omont 1985), if the spectrum has emission to be absorbed at the blueshifted edge of it, such as the blueshifted wing emission.

We roughly estimate an upper limit of the excitation temperature, and the lower limits of the optical depth and the mass of the absorbing cloud. A brightness temperature T_1 of the CO(J = 1–0) line, assumed to be an antenna temperature divided by the main beam efficiency, is expressed as

$$T_1 = T_0 e^{-\tau} + [J(T_{\mathrm{ex}}) - J(T_{\mathrm{bg}})](1 - e^{-\tau}) ,$$

at the self-absorption dip, where T_0 is a brightness temperature without the absorbing cloud, T_{ex} and τ are an excitation temperature and an optical depth of the absorbing cloud, respectively. $J(T) = h\nu/k \times [\exp\,(h\nu/kT) - 1]^{-1}$. Radio continuum emission from CRL 2688 is assumed to be negligible (Spergel, Giuliani, and Knapp 1983). T_{bg} is 2.8 K. From the formula we obtain ranges of T_{ex} and τ which satisfy the observed T_0 (=1.5 K) and T_1 (=0.5 K) to be lower than 4.8 K and higher than 1.2, respectively. The temperature obtained is at least 2 times lower than an excitation temperature of the central molecular envelope, 10 K. Using the derived excitation temperature and the optical depth, the lower limit of the H_2 column density is estimated to be $(0.7\text{–}2.0) \times 10^{18}$ cm^{-2} assuming the velocity width of 1.3 km s^{-1} and (CO)/(H_2) of 8×10^{-4} for T_{ex} = 3–5 K. If the absorbing cloud has a spherical shell with a radius of 0.6 pc, a lower limit of the mass is calculated to be $(1.8\text{–}4.4) \times 10^{-2}\ M_\odot$.

Since the emission from the central envelope is seen at a radius of 60″ (0.3 pc) (see Fig. 5), it is more likely assumed that the absorbing envelope surrounding the warm central envelope has a larger size (more than 1 pc) and a considerable mass (about $10^{-1}\ M_\odot$).

We are pleased to thank Drs. T. Hasegawa, M. Tsuboi, and S. Cho for valuable discussion, and acknowledge the staff in Nobeyama Radio Observatory for operating the 45 m telescope.

REFERENCES

Beckwith, S., Beck, S. C., and Gatley, I. 1984, *Ap. J.*, **280**, 648.
Beckwith, S., Persson, S. E., and Gatley, I. 1978, *Ap. J.* (*Letters*), **219**, L33.
Crampton, D., Cowley, A. P., and Humphreys, R. M. 1975, *Ap. J.* (*Letters*), **198**, L135.
Knapp, G. R., and Morris, M. 1985, *Ap. J.*, **292**, 640.
Knapp, G. R., Phillips, T. G., Leighton, R. B., Lo, K. Y., Wannier, P. G., Wootten, H. A., and Huggins, P. J. 1982, *Ap. J.*, **252**, 616.
Lo, K. Y., and Bechis, K. P. 1976, *Ap. J.* (*Letters*), **205**, L21.
Morris, M. 1981, *Ap. J.*, **249**, 572.
Morris, M., Lucas, R., and Omont, A. 1985, *Astr. Ap.*, **142**, 107.
Ney, E. P., Merrill, K. M., Becklin, E. E., Neugebauer, G., and Wynn-Williams, C. G. 1975, *Ap. J.* (*Letters*), **198**, L129.
Nguyen-Q-Rieu, Graham, G., and Bujarrabal, V. 1984, *Astr. Ap.*, **138**, L5.
Sakashita, S., Hanami, H., and Umemura, M. 1985, *Ap. Space Sci.*, **111**, 213.
Spergel, D. N., Giuliani, J. L., Jr., and Knapp, G. R. 1983, *Ap. J.*, **275**, 330.
Thronson, H. A., Jr., and Mozurkewich, D. 1983, *Ap. J.*, **271**, 611.
Ulich, B. L., and Haas, R. W. 1976, *Ap. J. Suppl.*, **30**, 247.
Zuckerman, B. 1978, in *IAU Symposium 76, Planetary Nebulae: Observations and Theory*, ed. Y. Terzian (Dordrecht: Reidel), p. 305.
Zuckerman, B., Gilra, D. P., Turner, B. E., Morris, M., and Palmer, P. 1976, *Ap. J.* (*Letters*), **205**, L15.

EDWARD B. FOMALONT: National Radio Astronomy Observatory, Edgemont Road, Charlottesville, VA 22901

MASATO ISHIGURO, NORIO KAIFU, TAKASHI KASUGA, RYOHEI KAWABE, HIDEYUKI KOBAYASHI, KOICHI MORITA, SACHIKO OKUMURA, and NOBUHARU UKITA: Nobeyama Radio Observatory, Tokyo Astronomical Observatory, University of Tokyo, Nobeyama, Minamimaki, Minamisaku, Nagano 384-13, Japan